Link between subsonic stall and transonic buffet on swept and unswept wings: from global stability analysis to nonlinear dynamics

Frédéric Plante, Julien Dandois, Samir Beneddine, Éric Laurendeau, and Denis Sipp

Supplementary material

1. Separation Metrics

This section reports separation metrics for a set of base-flows obtained in this paper. The maximum backflow velocity in the x direction $min(V_x)$, the separation location x_s and the reattachment location x_r, the separation thickness measured in the direction normal to the wall h_s, the length of the separation area $l_s = x_r - x_s$ and the projection of the separation length in the direction normal to the inflow $l = l_s sin\alpha$.

Table 1 lists the metrics of the recirculation bubble of the NACA4412 base-flows at a Reynolds number of 350 000. In every base-flow a trailing edge type separation is observed. For the base-flow on the lower branch, two zones where the backflow velocity is high are obtained. One is near the leading edge, and the other near the trailing edge. Only the maximum of these two velocities is reported.

Table 2 lists some of the metrics of the separation zone for the base-flows of the OALT25 aerofoil at a Reynolds number of 3 million. In every case the recirculation is present from the shock wave to the trailing edge. However, for the lower angle of attack the recirculation is thicker at the shock foot and near the trailing edge. For this reason, two separation zone thicknesses (h_{s1} and h_{s2}) are reported. These two zones of the recirculation bubble can be seen in fig 1.

Table 3 reports the separation metrics of the NACA0012 base-flows at a Reynolds number of 10^7. For the specific case of Mach number of 0.3 and 0.4 a small recirculation bubble is obtained at the foot of a small shock wave near the leading edge. The metrics are reported for the second trailing edge type of separation. For higher Mach number, flow separation occurs at the shock foot. For the Mach number of 0.2, only a trailing edge type separation is obtained.

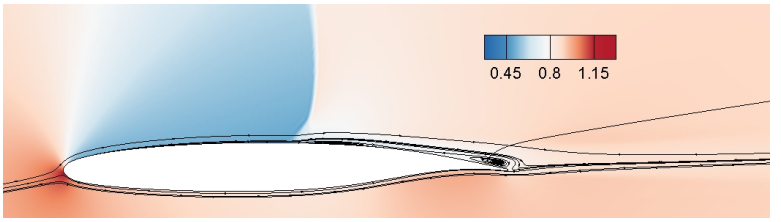

Figure 1: Density contours of the base-flow (OALT25, $M = 0.7352$, $Re = 3 \times 10^6$, $\alpha = 4.0°$, $\delta = 0°$).

α	δ	$min(V_x)$	x_s	x_r	h_s	l_s	l
14	0.	-0.163	0.618	1.	0.066	0.382	0.092
15.	0.	-0.187	0.518	1.	0.098	0.482	0.125
15.	10.	-0.186	0.518	1.	0.098	0.482	0.125
15.	20.	-0.184	0.527	1.	0.097	0.474	0.123
15.	30.	-0.180	0.538	1.	0.096	0.462	0.120
15.	40.	-0.174	0.562	1.	0.093	0.438	0.113
16.	0.	-0.203	0.434	1.	0.141	0.566	0.156
17.	0.	-0.209	0.351	1.	0.196	0.649	0.190
18.	0.	-0.210	0.286	1.	0.253	0.714	0.221
19.	0.	-0.208	0.212	1.	0.323	0.788	0.256
20.	0.	-0.205	0.146	1.	0.413	0.854	0.292
17. (lower branch)	0.	-0.265	0.100	1.	0.481	0.899	0.263
18. (lower branch)	0.	-0.244	0.108	1.	0.537	0.891	0.275
19. (lower branch)	0.	-0.225	0.005	1.	0.594	0.994	0.324
20. (lower branch)	0.	-0.220	0.004	1.	0.641	0.996	0.341

Table 1: Description of the recirculation bubble associated with the NACA4412 base-flows

α	δ	$min(V_x)$	x_s	x_r	h_{s1}	h_{s2}	l_s	l
3.5	0.	-0.115	0.563	1.	0.013	0.003	0.437	0.027
4.0	0.	-0.163	0.521	1.	0.024	0.007	0.479	0.033
4.0	10.	-0.160	0.521	1.	0.024	0.006	0.479	0.033
4.0	20.	-0.155	0.521	1.	0.024	0.006	0.479	0.033
4.0	30.	-0.146	0.521	1.	0.023	0.006	0.479	0.033
4.0	40.	-0.130	0.520	1.	0.023	0.005	0.480	0.033
4.5	0.	-0.212	0.480	1.	0.035	0.010	0.520	0.041
5.0	0.	-0.251	0.433	1.	0.047	0.014	0.567	0.049
6.0	0.	-0.301	0.338	1.	0.074	N/A	0.662	0.069
7.0	0.	-0.327	0.249	1.	0.105	N/A	0.751	0.092
8.0	0.	-0.341	0.162	1.	0.140	N/A	0.838	0.117
9.0	0.	-0.348	0.080	1.	0.181	N/A	0.920	0.144

Table 2: Description of the recirculation bubble associated with the OALT25 base-flows

Mach	α	$min(V_x)$	x_s	x_r	h_s	l_s	l
0.20	18.20	-0.189	0.581	1.000	0.061	0.419	0.131
0.30	15.00	-0.181	0.564	1.000	0.052	0.436	0.113
0.40	12.00	-0.169	0.544	1.000	0.051	0.456	0.095
0.50	7.90	-0.274	0.060	0.090	0.001	0.029	0.004
0.60	6.15	-0.215	0.163	0.226	0.002	0.063	0.007
0.72	3.50	-0.174	0.380	0.506	0.004	0.126	0.008

Table 3: Description of the recirculation bubble associated with the NACA0012 base-flows

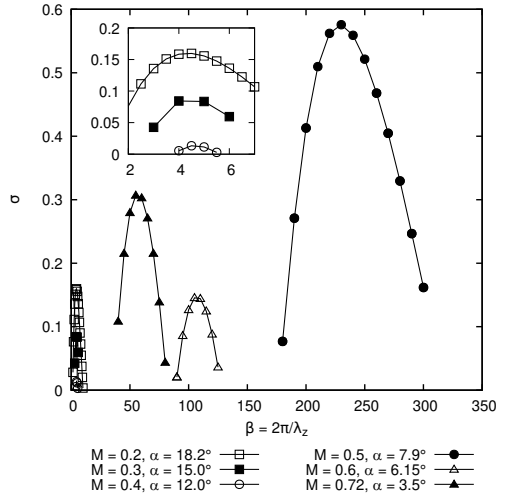

(a) Normalized by the chord length.

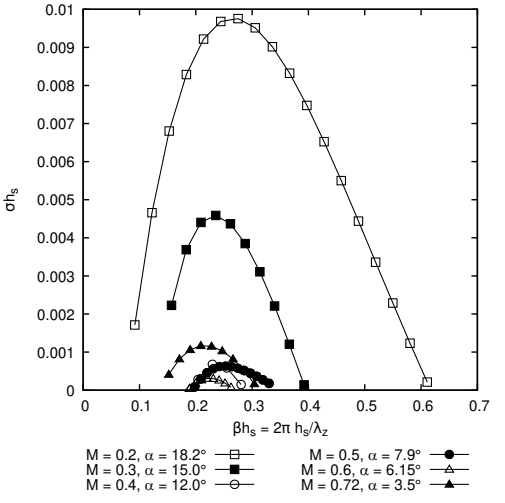

(b) Normalized by the separation height.

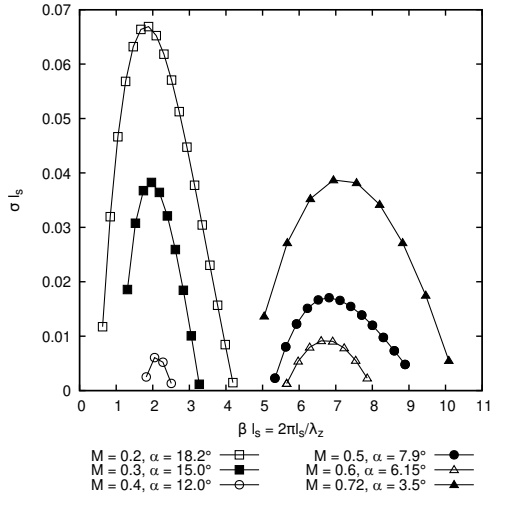

(c) Normalized by the separation length.

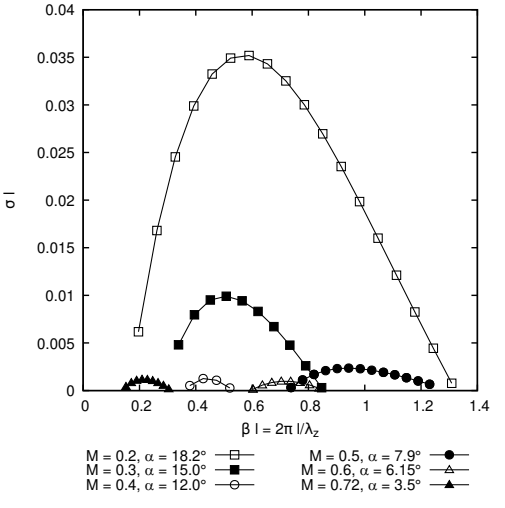

(d) Normalized by the projection of the separation length.

Figure 2: Effect of the Mach number and angle of attack on the growth rate of the three-dimensional mode (NACA0012, $Re = 10^7$, $\delta = 0°$).

2. Scaling of the 3D unstable modes

In the section 6 of the article, a scaling of the wavenumber of the stall and buffet cells by the separation height was proposed. Two other scalings were investigated, the scaling by the length of the separation l_s and projection of the separation length in the direction normal to the inflow l. These scalings are shown in fig. 2. By using the length of the separation, a proper scaling is obtained for the subsonic and transonic cases separately. But this scaling does not hold between these two flow regimes. The scaling by the projection of the separation length does not hold between Mach numbers.

For the case of the NACA0012 aerofoil, the height of the separation zone has been found to be a proper scaling to relate the size of the buffet cells and stall cells. Fig. 3 shows the application

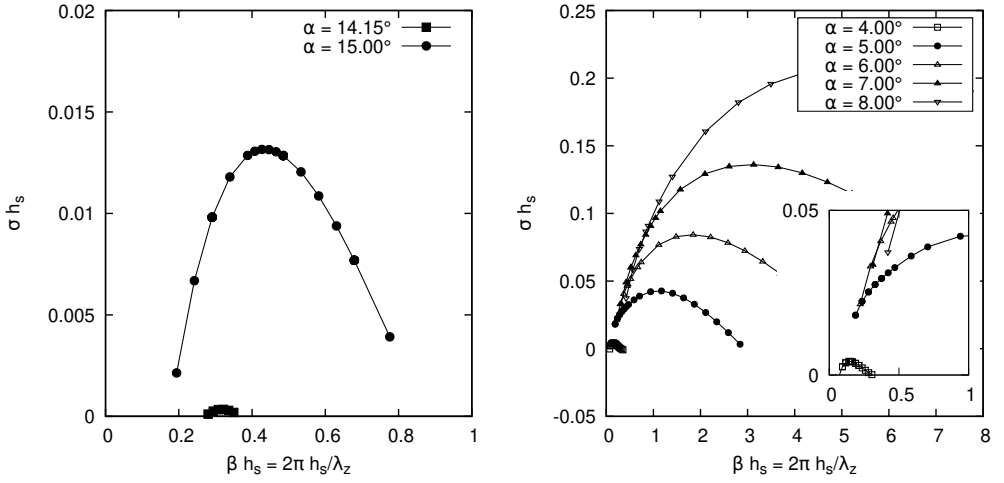

(a) NACA4412, $M = 0.2$, $Re = 350\,000$ and $\delta = 0.0$ (b) OALT25, $M = 0.7352$, $Re = 3 \times 10^6$ and $\delta = 0.0$

Figure 3: Scaling of the three-dimensional modes by the separation height.

of this scaling factor to the NACA4412 aerofoil in stall conditions and the OALT25 aerofoil in buffet conditions. The application of this scaling results in values of the normalized wavenumber βh_s around 0.3 and 0.2 for the NACA4412 and the OALT25 respectively at the onset of the instabilities.